

MEASUREMENT AND NUMERICAL SIMULATION OF THE TRANSIENT RESPONSE OF THE THICK-WALLED VESSEL.

MĚŘENÍ A NUMERICKÝ MODEL NESTACIONÁRNÍ ODEZVY TLUSTOSTĚNNÉ NÁDOBY.

Štefan Morávka*

The paper continues where the previous works finished. These works dealt with the experimental and numerical research of the transient elastic waves propagation in bodies with basic constructional forms (i.e. prism [8,10,11] and axisymmetric shafts [11,12,13,14] with variable shoulders, body with variable depth notches [11]). Next, the prism and circular plates with holes are ready for testing. The results of these works are required namely for the next development of the acoustic emission diagnostic method.

The aim of the presented work is to find the rules of the elastic wave propagation in a relatively more complicated body - more like a real structure. The thick-walled cylindrical vessel with the spherical bottom is modeled in the presented paper.

The experimental measurements were taken from the real specimen using the transient broadband piezoelectric sensor. The time responses of the vessel on the unit step force loading are measured. The results obtained from the experimental measurement are subsequently verified by confrontation with the results of the numerical computations using the Finite Element Method (FEM). The computational system MARC/MENTAT has been employed. The loading force imposes in the radial direction and that is why we are dealing with the 3D problem. The special 2D case is measured and solved too. In this case the loading force lies in the rotary symmetry axis.

Keywords: elastic waves, wave propagation, numerical modeling, finite element method, acoustic emission, piezoelectric transducer

1. BACKGROUND.

The acoustic emission (AE) signal rises in materials or structures, which are being loaded. It contains information about the emission source nature and emission site. This information propagates through the body and interacts with its surfaces. Then, the signal is taken from the body surface by the transducers with variable transfer characteristic. After that the signal is usually amplified and electronically processed. It is necessary to eliminate all these influences to be able to localize and characterize AE sources by return. To solve this inverse task we need to know the transfer characteristic of the used transducer among others, see e.g. earlier papers [1,4,9]. Then, we need to know the Green functions of the studied bodies and structures. We can get the Green's functions by calculation (numerical, analytical) or by experiment.

2. EXPERIMENTAL BODY AND MEASUREMENT.

The thick-walled (10 mm) cylindrical vessel ($\Phi 100/80$ mm, total height 200 mm) with the spherical bottom (see photo in fig.1 and scheme 2) is numerically and experimentally modeled in this work. It is required to understand the term "thick-walled" in the relation to the wave length which are considered namely. The vessel is made from usual structural steel class 11 (according to Czech norms).



Fig. 1. The photograph of the experimental body.

* Dr.Ing.Štefan Morávka, E-mail: moravka@ums.zcu.cz, New Technology Center of West Bohemia Region, Univerzitní 8, 301 16 Plzeň, Czech Republic, Phone: +420-19-7491-587.

The laboratory broadband piezoelectric non-resonance transducer designed according to [15] was employed for measuring of the vessel response. Various modifications of this transducer were modeled and its properties were studied in works [1,4,9].

The signals were generated by „pen-test“, i.e. by breaking of hard micro-lead. Six measurements were taken from each site and its arithmetic average was taken into account. The records are reproducible very well. It is not possible to realize the measurements at the inner curved surface of the vessel.

The digital oscilloscope TRACE with the higher sampling rate 40 MHz and with 8 bits resolution was employed for recording the data.

3. FEM MODEL AND COMPUTATION.

The body of the vessel is modeled from the homogeneous, elastic, isotropic material (steel). The excitation is realized by the unit force step – by unloading. In the 2D case the model is excited on the outer cylindrical surface in the direction of the symmetry axis. In 3D case the excitation has a radial direction and imposes on the place where the cylindrical and spherical surfaces transit, both see fig.2. 2D model consists of the 2,280 4-node plane izoparametric elements and it is computed with the 400 time increments. 3D model consists of the 21,848 8-node spatial izoparametric elements (the symmetrical half of model is considered) and 150 time increments are calculated. The computation ends with time 60 μ s, where the dilatation wave travels the path equal, approximately, to a double of the vessel height. We do not evaluate exactly in the term of the “Green function”, which describes responses on each excitation in each site, but we evaluate the response of the body in the specific suitable sites only (labeled point in fig.2). Secondly, we solve the response of vessel on the specific excitation – unit step only. But, we can determine the response on the general excitation using the convolution.

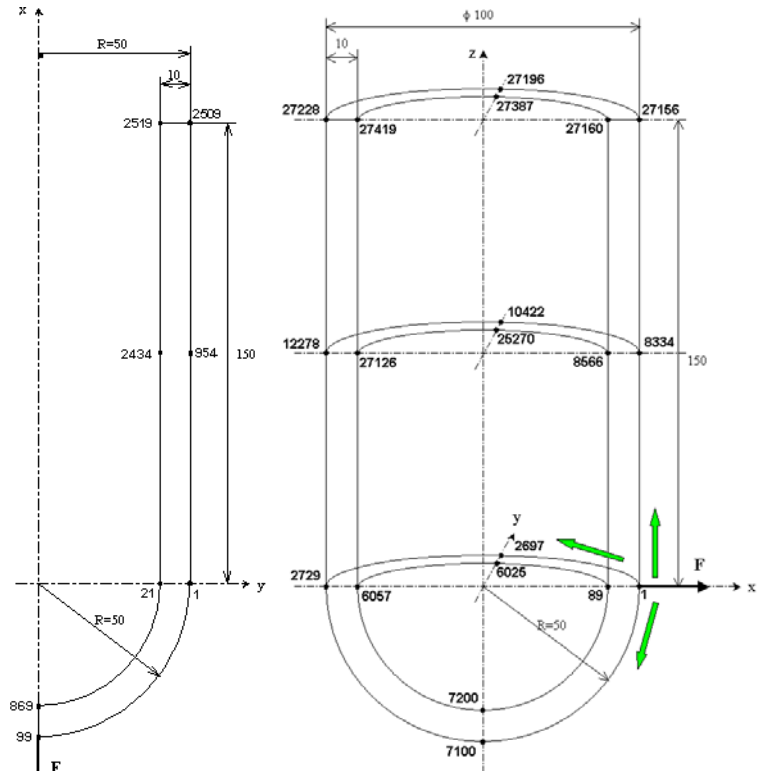


Fig. 2. The scheme of 2D and 3D FEM model of vessel with the excitation and pick-up sites. The arrows will be used below.

The good qualified choice of the integration method, the time integration increment and finite element size has fundamental influence on the quality of the results as well as on the technical costingness of a computation. This dilemma has been studied in the earlier papers dealing with the effects of the temporal and spatial discretization and its effects simultaneously, i.e. [5,6,7]. The former experience with choosing the parameter for calculations and comparisons of the numerical simulations and known analytical solutions has been taken into account too [2,3]. In the 2D case the elements with the 1 mm edge size were used. They are able to keep the frequencies approximately up to the 3 MHz (so-called cut-of-frequency) without the amplitude attenuation. The 2,5 mm sized elements, which are able to keep frequencies up to the 1.25 MHz, have been chosen in 3D case. The magnitude of time integration increment has been chosen in relation to the element size to get approximately the same frequency restriction as it is given by the choice of the finite element size. In the 2D problem $\Delta t = 0.15 \mu$ s and in 3D case $\Delta t = 0.4 \mu$ s.

The testing of 3D computation with the 5x5x2.5 mm elements was also realized to optimize the time consumption. In addition to the sizing up the elements the time increment was sized up 2 times. The results are similar. General differences follow – the curves computed by using the bigger elements have a half cut-of-frequency. This filter effect is more evident in the surrounding of the sharp curve changes. They become softer because of the absence of the higher frequencies. Second trend – the waves in a model with bigger elements propagate slower. This phenomenon is a natural (although undesirable) consequence of the temporal and spatial discretization. The explanation is given by the shape of dispersion curve (or area), which corresponds to the temporal discretization by the Newmark method, and spatial discretization with the consistent mass matrix, more i.e. in [2,3].

The Newmark method of the direct integration has been used with these coefficients $\beta = 0.275625$ and $\gamma = 0.55$. This choice, which surprises spurious effect of the higher frequencies namely, introduces the soft numerical dumping. At the same time it satisfies the unconditional stability of the method. The papers [2,3] were dealing with the suitability of this choice.

During measuring, we have been recording the frequencies up to 20 MHz. But, the curves still remain very steep. It would be better to choose lower time integration step and element size. What does it means? When we decrease element to a half size only, we get in 3D case 2^3 times more elements. The mass matrix has than 8 times longer edge and 64 times more elements. Then, the decreasing of the time increment is suitable too. Costingness and time consumption dramatically grows. Unfortunately, it is a big mistake to use different element size in the wave propagation computations, because the inhomogeneity is artificially introduced into continuum and the parasitic wave reflections appear on the boundary of unlike grids [2,3].

The computations were realized on the workstation SGI Octane with processor R10.000 and RAM 256 MB. The PC Pentium III 450 MHz, 512 MB was employed for tuning the tasks and design of grids. The FEM system MSC MARC/MENTAT was used. As it was written in the previous papers, if the computation runs “in-core” (in memory, without swapping), then PC can be in some cases up to 60% faster than the workstation! If we compare ratio cost/power than these machines differ multiply. It is obvious from this technical progress, why the PC software is not continuing to be only “cheaper derivation” of the workstation systems.

4. THE RESULTS OF EXPERIMENTS AND COMPUTATIONS ON 2D MODEL.

2D computation is a special case, where the modeling of a solid body with relatively small number of elements is possible. So, we are allowed to use smaller elements. There is only one possibility to realize 2D experiment - the excitation is laying in the rotary symmetry axis on the outer spherical surface. The inner spherical surface is accessible with difficulty.

Let as show some results. The first FEM result is in the fig.3 – the time dependence of axial displacement for the outer and inner surfaces in the place of the spherical and cylindrical surfaces transition. In time $t = 24.2 \mu s$, when the shear wave arrives, the curves diverge greatly-the wall is “bending”. Similar situation also duplicates “higher”- in the half of cylindrical surface height (nodes 954 and 2434).

In the figure 4 there is the same FEM computed time dependence of axial displacement on outer surface with the comparison with experimental measurement. We can see very good agreement of both curves. The crimp caused by Rayleigh wavefront in time $t = 26.1 \mu s$ is interesting. It is narrow, so it consists of high frequency components of spectrum. FEM computation with given parameters can reflect the slight undulation only. The shear wavefront arrives in monitored site in time $t = 24.20 \mu s$, if we take into account its trajectory on the outer surface. Considering the inner surface it arrives in time $t = 19.36 \mu s$. So, the peak near the time $t = 23 \mu s$ corresponds really with the shear wavefront. The difference around the $5 \mu s$ is consequence of the wall thickness in relation to the bottom curvature. The same effects appear in the middle of height and on the free end of cylindrical part (figs. unlisted here).

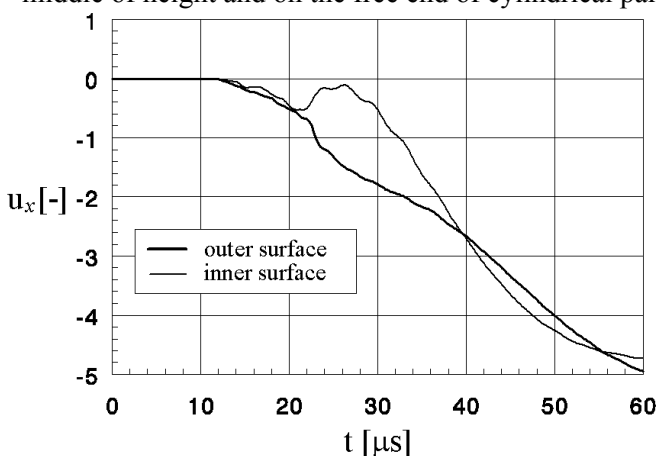


Fig. 3. The time dependence of the axial displacement of the outer and inner surfaces on the spherical and cylindrical part transition.

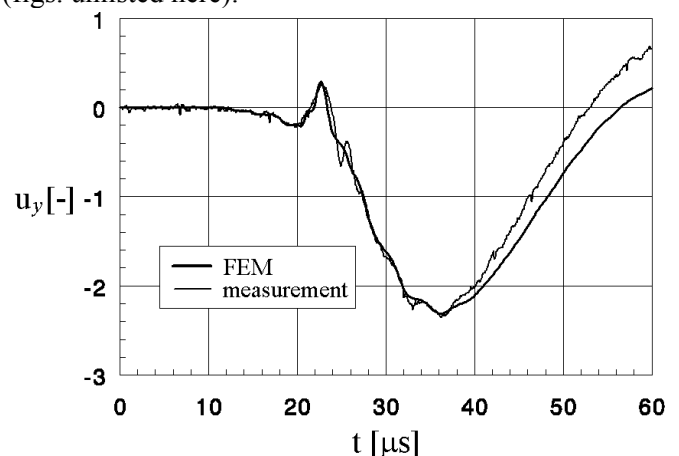


Fig. 4. The comparison of computed and measured time dependence of the axial displacement of outer surface on the spherical and cylindrical part transition.

The Results of Experiments and Computations on 3D Model.

Let us start with the illustrative example of excitement propagation of numerically computed distribution of radial displacement in time $t = 24 \mu\text{s}$, fig.5. The fig.6 shows the total displacement distribution in time $t = 52 \mu\text{s}$ at large displacement scale. The wave propagation and vessel deformation animations will be presented at the conference, if it is possible.

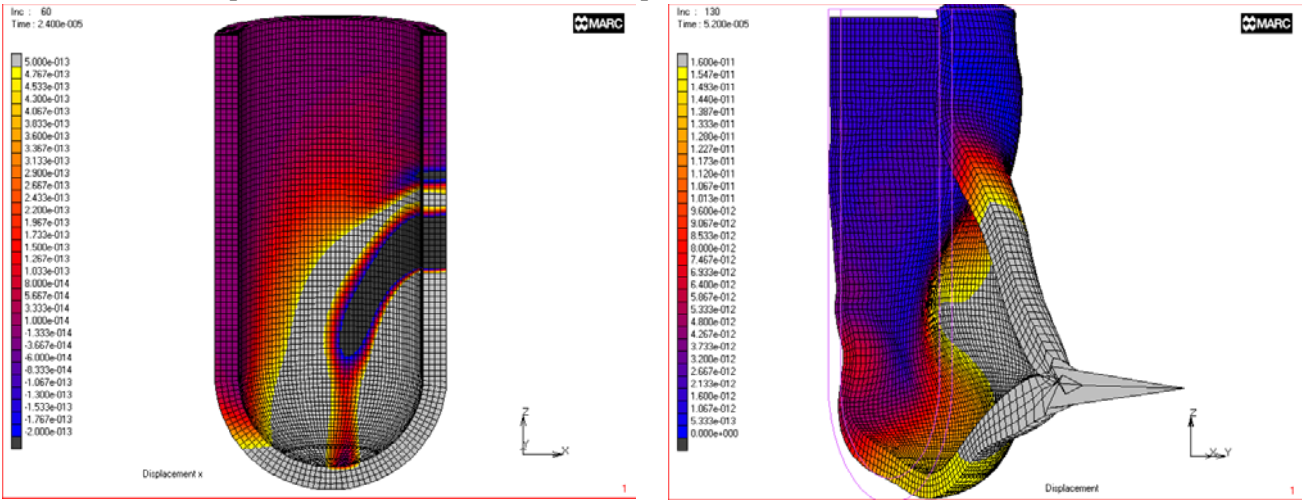
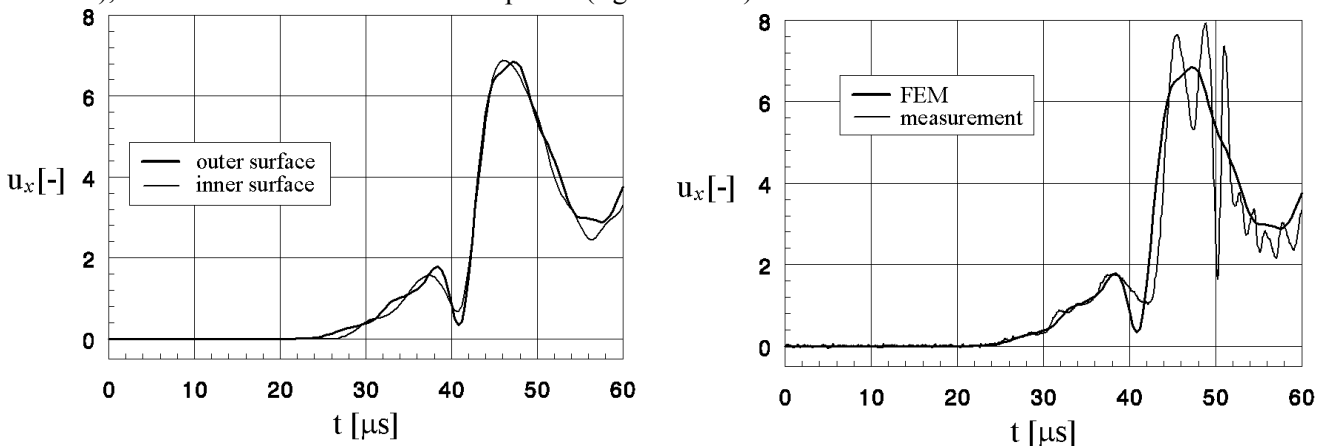


Fig. 5. Radial displacement distribution at $t = 24 \mu\text{s}$. **Fig. 6.** Total displacement distribution at $t = 52 \mu\text{s}$.

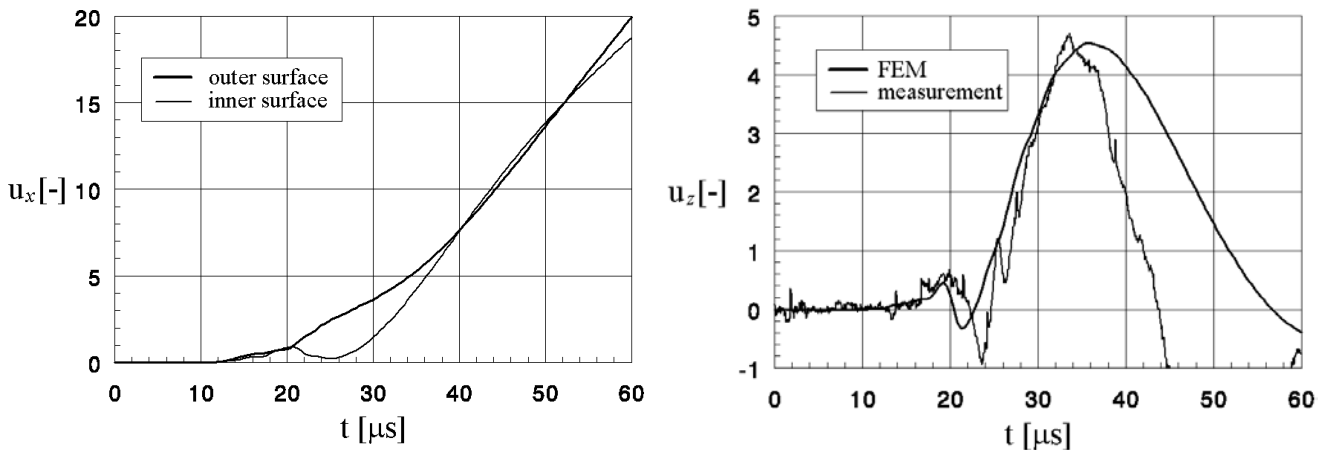
The curves of radial displacement on the spherical and cylindrical part transition in nodes 2729 and 6057 are shown in figs. 7 and 8. These nodes are opposite the exciting force. We are dealing with the course perpendicular to the wall and parallel to the initialization force, so that the “bending of the wall” does not happen here. The displacements of inner and outer surfaces are also not very different (similar to the site in a half of height of cylindrical surface “over” the force, nodes 8566 and 8334, not listed). But the difference from the experiment is bigger here. The measured curve is more oscillating than the frequency limited FEM computation. The agreement with the experiment is better in the site “above” this site (nodes 12278 and 27126), because the curves aren’t so steep here (fig. not listed).



Figs. 7 and 8. The time course of the radial displacement in nodes 2729 and 6057 on the inner and outer surface of the vessel. The comparison with the experiment on the outer surface.

In the figures 9 and 10 we follow the displacement courses on the “lowest” site of the vessel, in nodes 7100 and 7200. In the fig. 9 there is the course of the displacements parallel to the excitation force, tangential to the spherical surface here. The “bending” of the vessel wall (divergence of curves) appears here suddenly when the shear wavefront arrives in time $t = 24.2 \mu\text{s}$, as well as at the 2D model. The arrival time is computed using the longest way at the outer vessel surface. That is why we can see in the fig.9, that the wavefront arrives approximately $3 \mu\text{s}$ earlier than it responds to the trajectory in the middle of wall thickness. This phenomena does not appear at the axial displacement which is perpendicular to the surface, and the curves are very similar (fig. not listed). Next, the comparison of the computed and measured axial displacement at the outer surface is in the fig. 10. We can see here, that i.e. the fine oscillations in surrounding of Rayleigh wave front in time $t = 26.1 \mu\text{s}$ are not reflected by computation at all. The curves

become considerably different for a longer time. It can be caused by both dispersion phenomenon at the numerical computation and e.g. by discharging inner charge in transducers piezoelement.

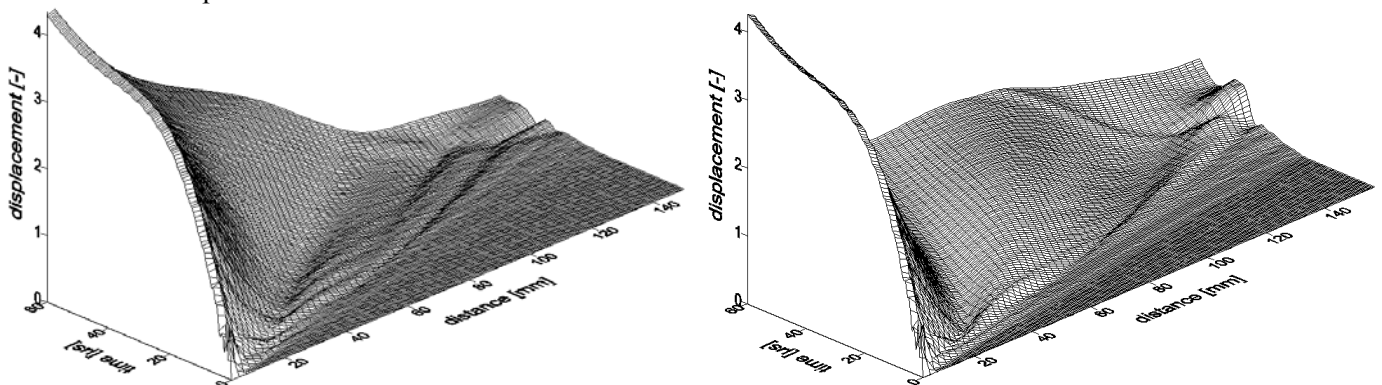


Figs. 9 and 10. The time course of the axial displacements in nodes 7100 and 7200 on the inner and outer vessel surface (tangential direction parallel to the excitation and the axial direction). The comparison with the experiment on the outer surface.

The courses at the spherical and cylindrical surface located 90 degrees from the excitation site (nodes 2697 and 6025) have the similar nature as the ones mentioned just above (fig. not listed). Only the phenomena of the “wall-bending” appears here in time $t = 24.2 \mu$ s for the displacement parallel to the excitation force (of course), tangential to the surface here. The level of agreement with the experiment is similar there as well. In the “combined” position “over” together with the “aside” to the excitation force (nodes 10422 and 25270) the “bending” appears too, but it is more complicated. The curves are crossing each other twice. The agreement with the experiment is very good here as well. (fig. not listed).

Let us present the summary results before the conclusion. They show the wave nature of the problem better. The time dependences of the total time displacements for the all points at lines rising from the site of excitation (see arrows in fig. 2) are shown. The first line is going straight on the cylindrical surface to the direction “up” from the excitation place up to the vessel edge (fig. 11). The second line is led by the semicircle “down” from the excitation place across the spherical surface up to the transition to the cylindrical surface (fig. not listed). The third line goes to the semicircle as well, but it follows the boundary of spherical and cylindrical surfaces (fig. 12).

The possibility to recognize the specific types of waves as at the simple bodies (namely prismatic, see [8,10-14]) is not good in these figures. All lines are led in the minimal trace, so that wavefront cannot be “drawn away”. There is a flat triangular area in the right down corner in the both figures. This area is not affected by wave process. The repeated glimmers or soft undulation are characteristic for the first graph, for the line in cylindrical surface. On the line on the spherical and cylindrical boundary we can see the shear (!) wavefront going from the contrary side. The wavefront ran around the vessel from the opposite direction. Surprisingly, it is not the Rayleigh wavefront which is slightly slower and in addition it propagates at the surface, i.e. by the longer trajectory. The computer animation is available as well. The movement of separate wavefronts is possible to follow there.



Figs. 11 and 12. The time dependence of total displacements of all nodes on lines marked by arrows in fig. 2.

5. CONCLUSIONS.

Especially, the Rayleigh wavefronts are possible to recognize in results (on the displacements perpendicular to surface better). They arrival times correspond to the wave propagation on trajectories at the body surface. The shear waves are very expressive. Their wavefront arrival is characteristic by the sudden change of the inner and outer surface displacements – the “bending” of the wall appears. The arrival times of the shear waves correspond to the trajectory in the middle of the vessel wall thickness. And, this is quite considerable difference at this thick-walled model.

The results of the FEM numerical simulations have been compared with the experiments. It confirms the credibility of measuring without the verification computations on one hand (e.g. practical application of AE measuring), and the credibility of computations when the testing bodies are not available or it is not possible to realize measuring (numerical modeling) on the other hand. Obtained agreement of the numerical simulations and the experiments is relatively very good. The differences are caused namely by the frequency limitation of FEM, which depends on the element and time integration step sizes. The differences are caused namely by the FEM frequency limitation and by the element and time integration step sizes. Due to this filter effect the FEM results are relatively smooth and they cannot contain the sharp changes either, e.g. here relatively high-frequency based Rayleigh wave fronts. The soft time shifts among the computation and experiment appears somewhere. It results from the dispersive properties of FEM used for the simulation of the transient effects.

The transient numerical computations are very computer demanding, and so, in our specifications, their possibilities are somewhat behind the measuring possibilities. But, all is changing very quickly...

6. LITERATURE.

- [1] Hora P. & al.: Nové metody vyhodnocování signálů akustické emise. *Závěrečná zpráva o řešení grantu GAČR č.101/94/0971, Plzeň, Západočeská univerzita, 1997.*
- [2] Morávka Š.: Porovnání analytického řešení nestacionární rázové napjatosti kontinua s výpočtem pomocí MKP., *Strojnícky čas.* 49, č.6, str.406-425, Bratislava, 1998.
- [3] Morávka Š.: Testování možností modelování nestacionárního šíření napěťových vln metodou konečných prvků. *Národní konference Inženýrská mechanika '98, str.489-494, Svratka, květen 1998.*
- [4] Morávka Š.: Analýza širokopásmového snímače napěťových vln. *Kolokvium Diagnostika a aktivní řízení '98, str.29-34, Brno VUT, listopad 1998.*
- [5] Morávka Š.: Společné posouzení vedlejších účinků časové a prostorové diskretizace při nestacionárním zatížení. *Národní konference Inženýrská mechanika '99, str. 391-396, Svratka, květen 1999.*
- [6] Morávka Š.: Disperze vln na MKP modelu způsobené současně časovou a prostorovou diskretizací kontinua. *Konference Výpočtová mechanika '99, str. 255-261, Západočeská univerzita, Nečtiny, říjen 1999.*
- [7] Morávka Š.: Side Effect of Simultaneous Spatial and Temporal Discretization of a Continuum Under Transient Load. *In: Proceedings of University of West Bohemia 1999, page 127-135, Plzeň, April 2000.*
- [8] Morávka Š.: The Elastic Wave Propagation over the Shape Transitions of Bodies. *International Conference Engineering Mechanics 2000, Svratka, page 133-138, Czech Republic, May 2000.*
- [9] Morávka Š.: The Analysis of the Broadband Transducer of Strain Waves, *38th International Conference EAN 2000, page 199-206, Třešť, Czech Republic, June 2000.*
- [10] Morávka Š.: Šíření elastických vln v prismatických tělesech se strmými změnami tvaru. *16. konference s mezinárodní účastí, Computational Mechanics 2000, str. 283-290, Nečtiny, Czech Republic, October 2000.*
- [11] Morávka Š.: Modelování šíření napěťových vln pro účely zpětné rekonstrukce zdroje akustické emise, *Závěrečná zpráva o řešení grantu GAČR č.101/97/P007, Plzeň, Západočeská univerzita, leden 2001.*
- [12] Morávka Š.: Numerical and Experimental modelling of the elastic wave propagation in the shafts with offsets. Affecting of measurements by transducer's presence. *National conference with international participation Engineering Mechanics 2001, p.177, Akademie věd ČR, Svratka, květen 2001.*
- [13] Morávka Š.: Porovnání numerického modelu šíření elastických vln v tělesech s výsledky měření piezoelektrickým snímačem. Vliv přítomnosti snímače na měření. *38th International Conference EAN 2000, pp.231-236, Tábor, June 2001.*
- [14] Morávka Š.: Šíření elastických vln v rotačně symetrických tělesech s tvarovými přechody - 3D MKP model a experiment. Zpětné ovlivnění měření přítomností snímače. *17.konference s mezinárodní účastí Výpočtová mechanika 2001, str.223-230, Západočeská univerzita, Nečtiny, listopad 2001.*
- [15] Proctor T. M. Jr.: An Improved Piezoelectric Acoustic Emission Transducer., *J.Acoust. Soc. Am., vol. 71, pp. 1163-1168, No. 5, 1982.*

This paper is based upon work sponsored by the Ministry of Education of the Czech Republic under research and development project LN00B084.